Sensors and Actuators B 201 (2014) 444–451

Contents lists available at ScienceDirect

Sensors and Actuators B: Chemical

journal homepage: www.elsevier.com/locate/snb

Review

Direct hydrothermal growth of ZnO nanosheets on electrode for ethanol sensing

Dianxing Ju, Hongyan Xu*, Jun Zhang, Jing Guo, Bingqiang Cao**

School of Materials Science and Engineering, University of Jinan, Shandong Provincial Key Laboratory of Preparation and Measurement of Building Materials, Jinan 250022, Shandong, China

ARTICLE INFO

Article history:
Received 6 December 2013
Received in revised form 31 March 2014
Accepted 21 April 2014
Available online 29 April 2014

Keywords:
Zinc oxide
Nanosheets
Hydrothermal
Gas sensor
Sensitivity

ABSTRACT

ZnO nanosheet microstructures have been directly grown on Al_2O_3 tube electrode by one-step hydrothermal method with different reaction times (3 h, 8 h and 12 h). The crystalline phase, morphology, and structure of the nanosheets are characterized by FESEM, TEM/SAED, and XRD. The results of FESEM reveal that ZnO nanosheets exhibit a sheet networks structure and a lager surface area. TEM/SAED images show a rough surface and a polycrystalline structure of ZnO nanosheets. X-ray diffraction indicated the ZnO architectures are well-crystallized in a hexagonal wurtzite structure. Gas sensing properties of the ZnO nanosheets show high response, fast response–recovery curves and long-term stability to 25–1000 ppm ethanol at appropriate temperature (400 °C), especially for sensor B (8 h). Moreover, the response of sensor B can get up to 38.4 for 100 ppm ethanol, and even 25 ppm ethanol could be well detected with a high response about 15 which is mainly attributed to the high surface area. This demonstrated the great potential application of ZnO nanosheets for developing gas sensors.

Contents

1. Introduction

For sensor applications, metal oxide semiconductors like SnO_2, ZnO and TiO_2 have been investigated for several decades [1–3]. Most of them are expected to be excellent candidates to fabricate gas sensors for detecting harmful target gases [3,4]. As a typical n-type metal oxide semiconductor, ZnO, with a wide band gap (3.37 eV) [5,6], shows good morphology tailoring properties, high electron mobility, good chemical stability and low production cost [7], which are all desirable characteristics for gas sensor. Previous reports have demonstrated that ZnO exhibits good response characteristics to many toxic gases like H_2S [8], NO_2 [9] and CO [10], especially for the nanostructures.

Due to high specific surface-to-volume ratio, one-dimensional ZnO nanostructures like nanowires [11], nanotube [12] and nanobelts [13] have been widely adopted to fabricate gas sensor. In 2007, Chen et al. [12] synthesized ZnO nanotubes by a sonochemical method at low temperature, exhibited better ethanol sensing properties at a working temperature of 300 °C. In 2012, Wang et al. [14] synthesized ZnO nanorods by a simple low temperature hydrothermal process, and the sensor exhibited a high, reversible and fast response to ethanol. Generally, these sensors are assembled by two steps. First, ZnO nanostructures are synthesized

* Corresponding author. Tel.: +86 531 89736292; fax: +86 531 87974453.
** Corresponding author.
E-mail addresses: mse_xuhy@ujn.edu.cn (H. Xu), mse_caobq@ujn.edu.cn (B. Cao).

http://dx.doi.org/10.1016/j.snb.2014.04.072
0925-4005/

by different methods like hydrothermal method [15,16], metal organic chemical vapor deposition (MOCVD) [17], and pulsed laser deposition (PLD) [18]. Then the obtained ZnO samples need to be collected or peeled off from substrates and ground to form homogenous paste that could be coated onto the alumina ceramic tubes. Obviously, such a sensor fabrication process is time-cost and sometime will destroy the intrinsic nanostructure properties. In 2007, Bie et al. [19] prepared ZnO nanorod arrays directly on Al_2O_3 tube through a two-step solution method, which simplified the traditional two-step process of sensor fabrication. However, the poor contacts between the vertical nanorods and Al_2O_3 tube limited the movement of electrons, increased the device resistance and further reduced the sensor sensitivity.

Two-dimensional (2D) nanostructures such as ZnO nanosheets [20] and nanoplate [21] have provided good opportunities to explore new physical and chemical applications of nanostructures with different dimensionalities. From the practical point of view, ZnO nanosheet networks are extremely interesting because of their large surface areas and better conductivity, which have potential practical application in sensors, solar cells [22], UV photodetectors [23], and field emission devices [24]. In comparison to nanowires, the growth of 2D ZnO nanostructure is much more difficult partially due to its hexagonal polar structure. The basal plane of (0 0 0 1) has the highest surface energy that induces the fast growth along the *c*-axis direction with the result of preferred 1D nanowire growth [25]. Till now, only a few papers have reported the growth of ZnO nanosheets. Rahm et al. [26] reported the synthesis of ZnO nanosheet networks with carbothermal reduction on sapphire substrates using gold as catalyst via the well-known vapor–liquid–solid (VLS) mechanism. Recently, Zhang et al. [27] successfully synthesized porous ZnO nanosheets with a hydrothermal method by annealing of the zinc carbonate hydroxide hydrate precursors and demonstrated their ethanol response through a traditional gas sensor fabrication process. Therefore, how to grow ZnO nanostructures directly onto the generally used alumina ceramic Al_2O_3 tubes for gas sensor application is still a big challenge.

In this work, we simplified the traditional two-step process of sensor fabrication and report a one-step, cost-effective and environment-friendly hydrothermal approach for first synthesizing ZnO nanosheet networks on ordinary alumina tube and their application for gas sensors. The seed layer percolating step is proved to be crucial for the ZnO nanosheets direct growth on the alumina tube. The influence of reaction time on the growth of such ZnO nanosheet network was also investigated. The primary optimized ZnO nanosheet sensors assembled by such a direct one-step growth exhibits better sensing properties in comparison with isolated ZnO sensors. The larger surface area of ZnO nanosheet network may give a relatively simple account of the improved the sensor performance.

2. Experimental

ZnO nanosheets were synthesized through one-step, low temperature (95 °C) hydrothermal process [19,27]. All the chemicals were used as received (Sinopharm Chemical Reagent) without further purification. The typical process was described as follows: 2.7 g $Zn(Ac)_2$ was dissolved in 125 mL ethanol and heated under reflux at 95 °C until the $Zn(Ac)_2$ was completely dissolved, and then the ZnO sol was obtained after LiOH was added into the above solution. Cleaned Al_2O_3 tubes (4.0 mm in length, 1.0 mm in internal diameter and 1.4 mm in external diameter) with a pair of Au electrodes (2.0 mm in distance) attached with Pt lead wires (as shown in Fig. 2), were immersed into the ZnO sol for a period of time and annealed at 350 °C for 30 min to grow a ZnO seeds layer. Mixed aqueous solution of 0.025 M zinc nitrate and 0.025 M hexamethylenetetramine ($C_6H_{12}N_4$) was transferred into Teflon-lined stainless steel autoclaves and the Al_2O_3 tubes were suspended in the aqueous solution at 95 °C and then ZnO nanosheets were grown directly on the Al_2O_3 tube from the chemical reaction [19]:

$$2Zn(NO_3)_2 + C_6H_{12}N_4 + 8H_2O \rightarrow 2ZnO + 4NH_4NO_3 + 6HCOH \quad (1)$$

After the reaction at 95 °C for 3 h, 8 h and 12 h, we got three groups of ZnO samples, named as sensor A, B, C, respectively. The samples were rinsed with deionized water and absolute ethanol for several times and then dried in air for further characterizations.

The morphology, structure and crystalline phase of the ZnO nanosheets films were characterized by field emission scanning electron microscope (FESEM, Quanta FEG250), transmission electron microscopy/selected area electron diffraction (TEM/SAED, JEM-2100F, JEOL), and X-ray diffraction (XRD, D8-Advance, Bruker) with Cu Kα radiation. The gas-sensing performance of ZnO nanosheets was measured through a gas-sensing characterization system (WS-30A, Weisheng Electronics Co., Ltd., China). The concentrations of the target gases were obtained by the static gas distribution method, which was calculated by the following formula [20,28]:

$$Q = \frac{V \times \varphi \times M}{22.4 \times d \times \rho} \times 10^{-9} \times \frac{273 + T_R}{273 + T_B} \quad (2)$$

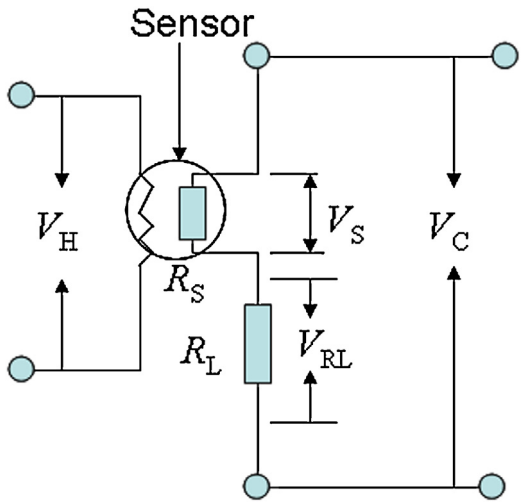

Fig. 1. Electronic circuit of gas sensor measurement system. V_H is the heating voltage, R_L is a constant resistance (4.7 MΩ), V_{RL} is the voltage on R_L and V_C is the constant voltage (5 V) which is applied on the R_L and the sensor.

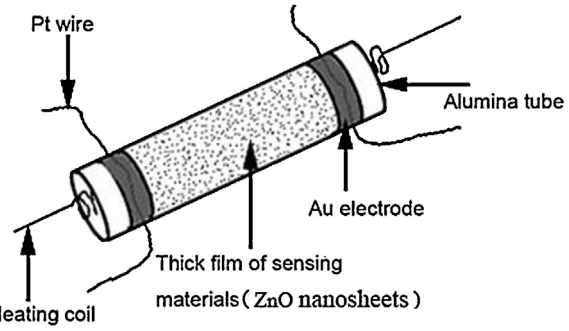

Fig. 2. Schematic drawing of a sensor element. Al_2O_3 tubes (4.0 mm in length, 1.0 mm in internal diameter and 1.4 mm in external diameter) with a pair of Au electrodes (2.0 mm in distance) attached with Pt lead wires.

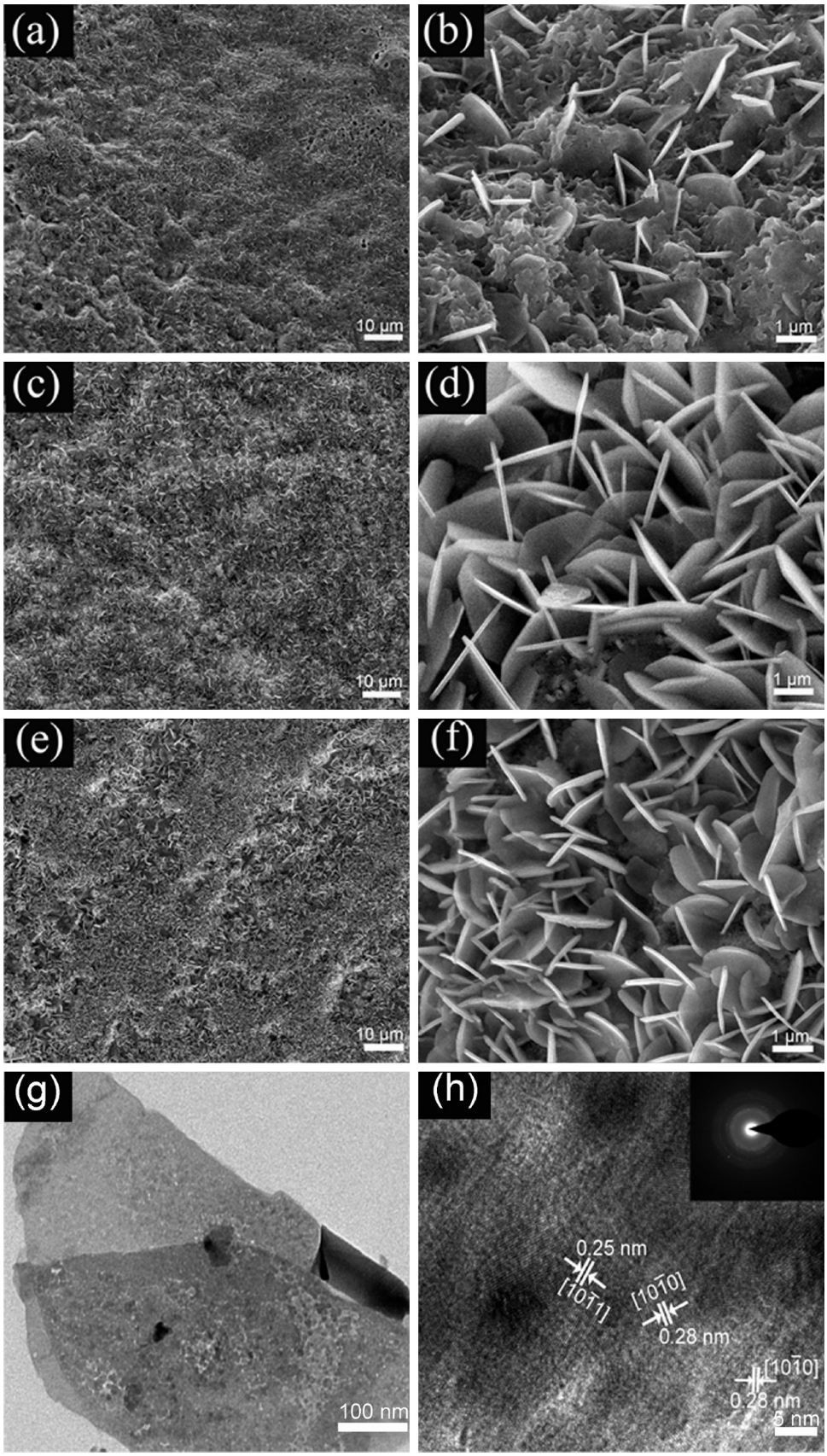

Fig. 3. (a–f) FESEM images of ZnO nanosheets with the reaction time (a, b) 3 h; (c, d) 8 h; (e, f) 12 h; (g, h) TEM and HRTEM images of ZnO nanosheets.

where Q (mL) is the liquid volume of the volatile compound, V (mL) is the volume of the testing chamber, φ is the required gas volume fraction, M (g mol^{-1}) is the molecular weight, d (g cm^{-3}) is the specific gravity, and ρ is the purity of the volatile testing liquid, T_R and T_B (°C) are the temperatures at ambient and test chamber, respectively. Ethanol, isopropanol, benzene and xylene vapors were used as the testing gas. The electronic circuit is shown in Fig. 1. In the circuit, V_H is the heating voltage, R_L is a constant resistance (4.7 MΩ), V_{RL} is the voltage on R_L and V_C is the constant voltage (5 V) which is applied on the R_L and the sensor. Then the sensor response is defined as follow: $S = R_a/R_g$, where R_a and R_g are the resistance of the gas sensor in air and in testing gas.

3. Results and discussion

3.1. Crystal structure and morphology of the ZnO nanosheets

The sample morphology was characterized by FESEM as shown in Fig. 3. Fig. 3(a) and (b) is FESEM images of ZnO nanosheets prepared with the hydrothermal method for 3 h. It shows rare and almost isolated nanosheets grown on the surface of the Al_2O_3 tube which may cause a large resistance and a poor conductivity. Fig. 3(c) and (d) is grown with 8 h. It can be found obviously that the nanosheets are uniform and homogenous with a large size and density. Most of the nanosheets stand uniformly on the substrate and connect with each other to form a network. Fig. 3(e) and (f) is the SEM images of ZnO nanosheets grown with the reaction time of 12 h. Compared with Fig. 3(c) and (d), they have larger density which may limit the growth of the nanosheets. As a result, the size of nanosheet is generally smaller. Fig. 3(g) shows the TEM image of the ZnO nanosheet with a rough surface. It can be seen clearly that the structure of ZnO nanosheet is polycrystalline and composes of numerous grains in nanoscale. Fig. 3(h) shows the HRTEM images of the nanosheet. It further proved the polycrystalline structure combined with the SAED (the inset of Fig. 3(h)). In addition, the lattice spacing of a nanoparticle is determined to be 0.28 nm and 0.25 nm, corresponding to the distance between two {10-10} (equivalent plane (01-10)) and {10-11} planes of the wurtzite ZnO. Moreover, larger numbers of nanoparticles present the lattice spacing of 0.28 nm than others, which means that there are numerous grains are along the {01-10} crystallographic directions within the {0 0 0 1} planes. Nevertheless, by introducing a seed layer, 2D ZnO nanosheets network was successfully grown on the Al_2O_3 tube via a one-step hydrothermal method for sensor fabrication. The rough surface of nanosheet and porous structure between nanosheets increases the specific surface area and the interconnected network offers good pathway for electron moving. These two characteristics are both preferred for high sensitive sensors.

Generally, based on the surface energy minimization in the solution system, the intrinsic structure of ZnO crystallite determined their fastest growth and spurs it to grow along the *c*-axis, and thus, the rod-like morphology is much more favorable in the thermo-dynamic equilibrium state. In addition, the growth of ZnO crystallite is also influenced by the external growth conditions such as pressure, pH value, temperature and growth time [29]. For example, Bie et al. [19] prepared ZnO nanorod arrays directly on Al_2O_3 tube through a two-step solution method. According to it, we obtained the ZnO nanosheets by changing the external growth conditions (hydrothermal method), Thus, a possible mechanism for the ZnO nanosheets has been put forward. In the case of the growth of ZnO nanosheets, ZnO seed-layer is firstly formed before hydrothermal process through the calcinations to form nucleation, which serves as the lattice-matched template for the growth of ZnO nanosheets. In the process of hydrothermal growth, a large quantity of ZnO nuclei are formed and aggregated when the degree of super saturation exceeds its critical value. Because of the high pressure, the growth direction along the *c*-axis is restrained, which lead to a non-equilibrium growth of the ZnO crystalline, and the growth rate changes to $V\{01\text{-}10\} > V\{0\,0\,0\,1\}$ [20,30], and further form the sheet-like morphology.

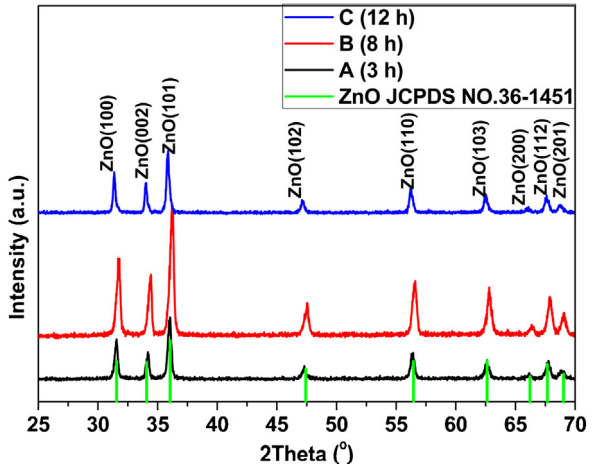

Fig. 4. XRD patterns of ZnO nanosheets grown with three reaction times as shown in brackets.

The crystal structures of the ZnO nanosheets were characterized via XRD (as shown in Fig. 4). It can be found that all the characteristic peaks of the ZnO nanosheets match well with the diffraction pattern of typical hexagonal wurtzite ZnO structure (JCPDS Card No. 36-1451) and no peaks are observed for other impurities such as $Zn(OH)_2$ and zinc, indicating the growth of pure ZnO nanosheets and further calcination process is not needed [31,32].

3.2. Sensing properties of the ZnO nanosheet

All the experiments were carried out with the relative humidity lower to 21%. It can be seen that there was little effect of the gas sensing properties with the relative humidity in this range, as shown in Fig. 5(a). In addition, some papers have also shown that the effect will be little with a lower relative humidity [33–35]. The first gas sensing properties of the ZnO nanosheets were evaluated determining the repeatability of the gas sensor. Fig. 5(b) indicates a typical response profile to investigate repeatability of the gas sensors after aged 3 days. It can be noted that all the sensors are in good reproducible run after five cycles, which demonstrated a better repeatability of the sensors. After aged two weeks, we determined the optimum operating temperature of the sensors. Fig. 6 shows the response of the different sensors to 100 ppm ethanol as a function of the operating temperature in the range of 220–420 °C. All of the sensors have a low response when the temperature is below 220 °C. But the response continuously increases and reaches its maximum at 400 °C which correspond with Refs. [27,36,37], and then rapidly decreases as the temperature further increased. This might be attributed to the competing desorption of the chemisorbed oxygen [19]. When the working temperature is higher than 400 °C, the chemical adsorption oxygen absorbed on the surface of the ZnO nanosheets will gain enough energy to desorb from the surface of ZnO nanosheets, and then the chemical adsorption oxygen get the saturation. With the increase of operating temperature, the rate of desorption is much higher than that of adsorption, limited the reaction between adsorption oxygen and target gas molecules and further reduced response. The response of sensor B (8 h) can get up to 40–100 ppm ethanol at the optimal working temperature and it is better than other sensors, as shown in Table 1.

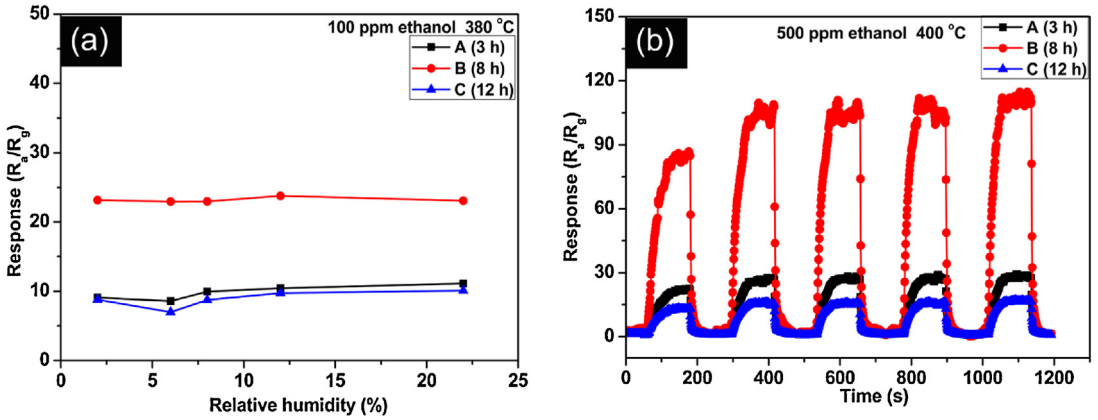

Fig. 5. (a) The relationship between response and relative humidity; (b) the repeatability testing of the sensors to 500 ppm ethanol at 400 °C with the relative humidity of 5%.

Table 1
Gas responses to C_2H_5OH of the ZnO nanosheets sensors in the present study and those reported in the literature.

Sensing materials (preparation)	[C_2H_5OH] (ppm)	R_a/R_g	T_{sens} (°C)	Refs.
ZnO nanorods (solution growth)	500	31	350	[19]
ZnO hierarchical nanostructures (microwave solution growth)	100	9	350	[21]
ZnO nanorods and nanoparticles (chemical precipitation)	250	25	400	[36]
ZnO nanoparticles (solution growth)	100	12	400	[38]
ZnO hierarchical nanostructures (emulsion-based solution growth)	100	177	400	[39]
ZnO nanowires (thermal evaporation)	100	1.7	300	[40]
ZnO tetrapod nanowires (thermal evaporation)	500	5.5	300	[41]
ZnO nanosheets (hydrothermal method direct on Al_2O_3 tube)	100	40	400	Our work

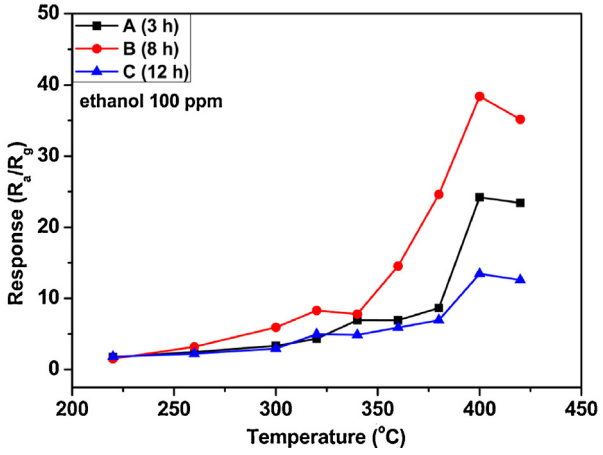

Fig. 6. Relationship between the response of the gas sensors and working temperature to 100 ppm ethanol with the relative humidity of 3–7%.

The response–recovery behavior is an important characteristic of gas sensors. Fig. 7 represents the sensors response–recovery behavior (a–c) and response (d) to different ethanol concentrations from 25 to 1000 ppm at 400 °C. When the sensors are exposed to the ethanol gas, the resistance of all the sensors shows a dramatic and sharp decrease and then reaches its equilibrium. Once the target gas is removed, the resistance of the sensors recovers rapidly to the baseline. In addition, all of them show that with the increasing of ethanol concentration, the ZnO nanosheets can adsorb more target gas molecules and exhibit higher response. Fig. 7(d) illustrated the response of the three gas sensors. It is obviously that the sensor B (8 h) exhibits higher response than others for higher ethanol concentration in the range of 25–1000 ppm, which can be attributed to the larger effective surface area of the ZnO nanosheets. Compared with the ZnO seed layer, shown in Fig. 7(e), the response of the three sensors is higher than that of ZnO seed layer which demonstrates a dominance of ZnO nanosheets.

As a typical n-type metal oxide semiconductor sensor, the ZnO based sensor belongs to the surface-controlled type, and the mechanism can be explained by the space-charge layer mode [42], which involves the formation of a charge depletion layer in the near-surface region of each grain, relative to the interior parts, due to electron trapping on adsorbed oxygen species [43]. The electrical conductance of the ZnO nanosheets sensor is determined by the amount of electrons in its conduction band. Thus, due to the larger effective surface area than other two sensors (sensor A and C), it offers numerous absorption site to absorb more oxygen molecular and form more $O^{\delta-}$ (O^{2-}, O^-, O_2^-) oxygen negative ions species by capturing electrons from the conductance band. When the oxygen negative ions react with ethanol, it will release more electrons to the conduction band of the nanosheets, and reduce the resistance of the sensor which exhibits a high sensitivity than others.

The sensing mechanism of the ZnO nanosheet sensors to ethanol can be explained as follows [14]: the oxygen vacancy in the ZnO nanosheets acts as an electron donor to provide electrons to conduction band of ZnO. When the ZnO nanosheet is exposed to air, oxygen molecules will be adsorbed on the surface of it to form $O^{\delta-}$ (O^{2-}, O^-, O_2^-) oxygen negative ions species by capturing electrons from the conductance band (Fig. 8a and b). It will form a depletion region [44], leading to an increase of the sensor resistance.

After the reductive ethanol is injected into the texting box and the sensors are exposed to ethanol vapor at a moderate temperature, the adsorbed ethanol molecules react with oxygen negative ions and release electrons by two reactions, and ethanol decomposes to acetaldehyde and hydrogen or to ethylene and water [45,46]. The decomposition of ethanol molecules depends on the acid–base properties of sensing materials [47]. Thus, the process of the dehydrogenation is depicted in Eqs. (3) and (4):

$$C_2H_5OH(g) \rightarrow CH_3CHO(g) + H_2(g) \quad (3)$$

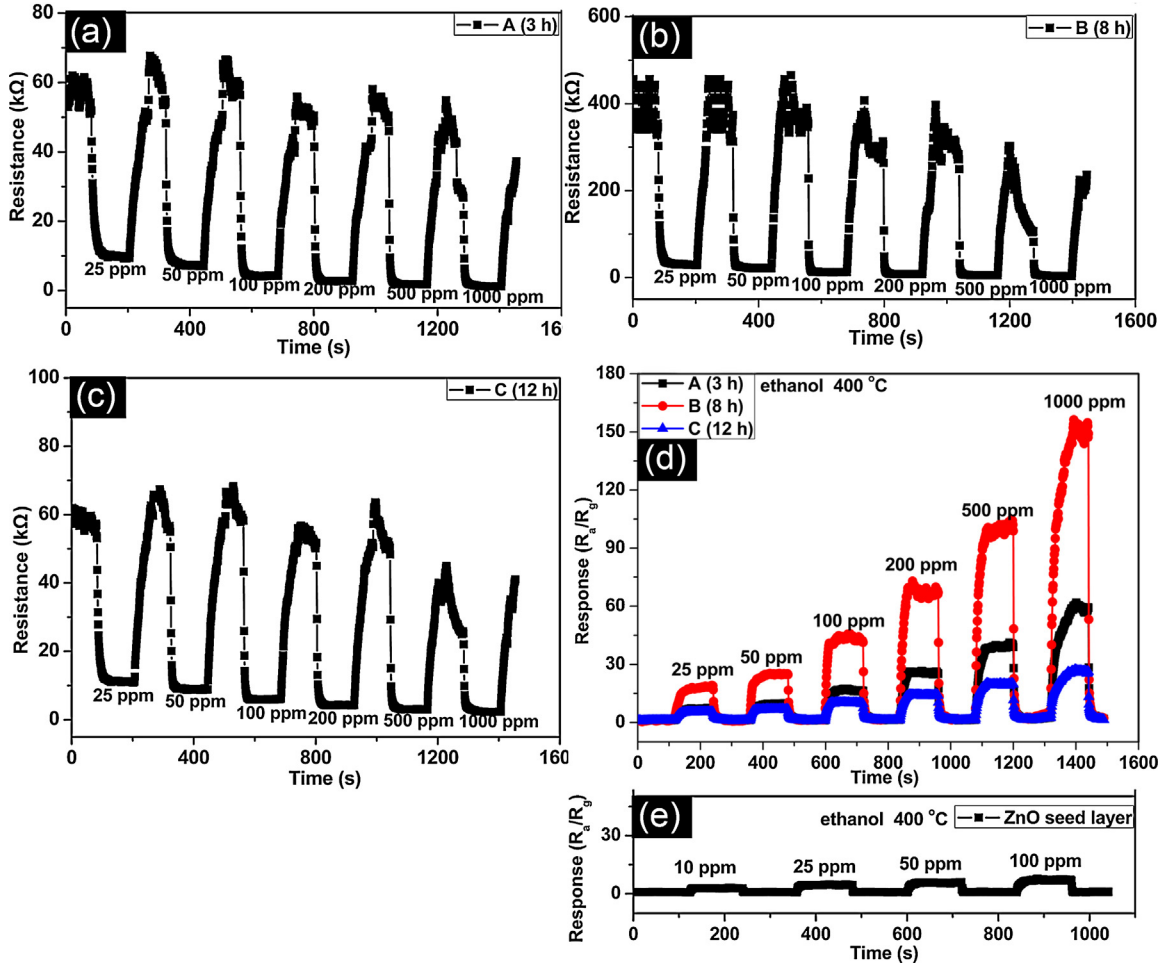

Fig. 7. (a–c) Response–recovery curves of sensors A, B, C to different ethanol concentrations at 400 °C; (d–e) relationship between response and different concentrations of ethanol at 400 °C.

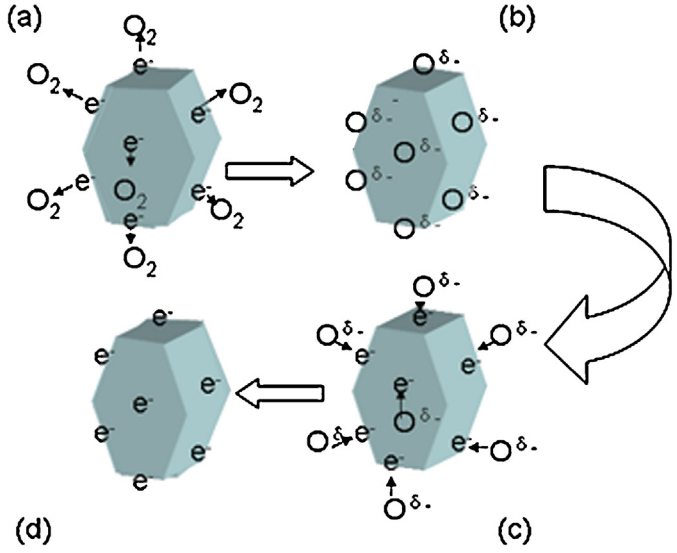

Fig. 8. Schematic illustration for the sensing mechanism of the ZnO nanosheets sensor to ethanol: (a) exposed to air; (b) $O^{\delta-}$ ions adsorbed; (c) exposed to ethanol; (d) release electrons to nanosheets.

$$C_2H_5OH(g) \rightarrow C_2H_4(g) + H_2O(g) \quad (4)$$

$$CH_3CHO(ad) + 5O^- \rightarrow 2CO_2 + 2H_2O + 5e^- \quad (5)$$

And then, the intermediate of $CH_3CHO(g)$ is subsequently oxidized to form CO_2 and H_2O, as depicted in Eq. (5), and release electrons back to the conduction band of the nanosheet, reducing the number of surface adsorbed oxygen species, as shown in Fig. 8(c) and (d). Consequently, the depletion layer on the surface of ZnO nanosheet becomes thin and the electrical conductivity of the sensors increases which exhibit a decrease of the sensor resistance [48,49]. Based on the formula of response ($S = R_a/R_g$), it shows a high sensitivity. According to Fig. 1, the circuit voltage (V_c) is constant, so when the resistance of the sensor decreased, it will leads to the increase of the circuit current. As a result, the output signal voltage increases. When the ZnO nanosheets sensors are exposed to the oxidative gas, such as NO_2, an opposite electrical behavior can be observed.

The selective capacities of the sensors based on the ZnO nanosheets are tested to various gases at 400 °C, as shown in Fig. 9(a). It can be found that sensors A and B exhibit better selectivity to ethanol than sensor C. However, a phenomenon should be noted that the sensors response to ethanol is higher than to isopropanol. Generally, the hydrocarbon chain of isopropanol is longer than that of ethanol which suggests that the negative charge of oxygen atom would increase with the increase of the electron donating effect of the hydrocarbon chain. This will enhance the response of the sensor. However, as to ethanol and isopropanol, the volume of former molecule is smaller than the latter, which is convenient for the adsorption of ethanol molecule when the multi-layers exposed to the test gases. As a result, the sensors adsorb more ethanol molecules than isopropanol molecules, resulting in a higher effect

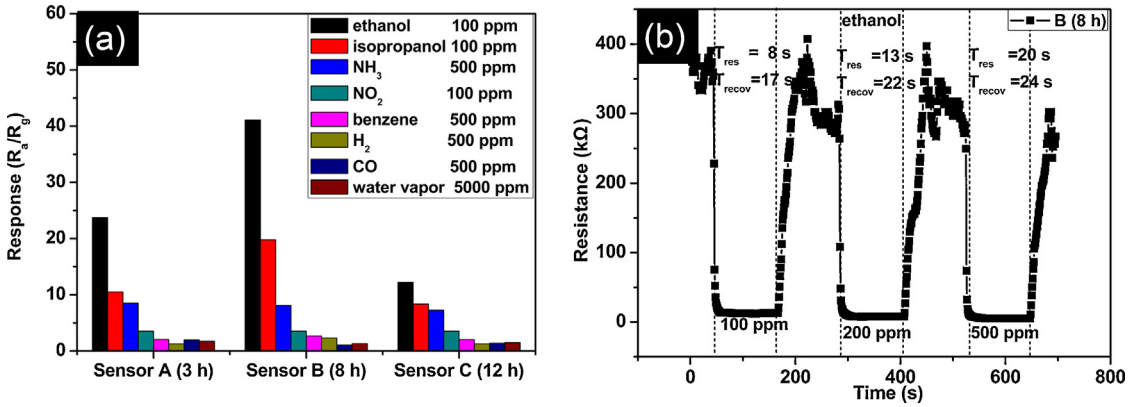

Fig. 9. (a) Selectivity of the three sensors (A, B, C) to different vapors at 400 °C with the relative humidity of 3–6%; (b) response–recovery times to different ethanol concentrations at 400 °C.

than electron donating effect of isopropanol molecule, and leading to a higher response to ethanol than to isopropanol [50,51]. In addition, sensor B (8 h) exhibits a good response–recovery property, as shown in Fig. 9(b). It shows a response–recovery curve to ethanol with different concentrations. The response and recovery time were defined as the time taken by the sensor to achieve 90% of the total resistance change in the case of adsorption and desorption, respectively. The observed have been found to be similar to that predicted earlier [52,53], where it is clear that with the increase of the ethanol concentration, the response and recovery time increase. This may be attributed to the diffusion of ethanol gas molecular. The more the ethanol gas molecules are provided, the longer the response and recovery time will be.

4. Conclusions

In summary, ZnO nanosheets with hierarchical structure grown directly on the Al_2O_3 tube substrate, exhibiting accessible surface, can be gained through a facile one-step hydrothermal method which simplifies the gas sensor fabrication process. ZnO seed-layer firstly covered on the Al_2O_3 tube substrate acts as the lattice matched template. We got a better sample with larger surface area and density of nanosheets by regulating the reaction time. The sensing properties showed that sensor B (8 h) has higher response at appropriate temperature (400 °C), especially to reducing ethanol vapor. The response could reached to 38.4 for 100 ppm ethanol which demonstrating its greater potential application as a gas sensor to detect reducing ethanol vapor.

Acknowledgments

This work is supported by NSFC (11174112) and Shandong Provincial Science Foundation (JQ201214, BS2012CL003, and BS2010CL007). The research programs from Ministry of Education of the People's Republic of China are also acknowledged (NCET-11-1027, 213021A). BC thanks the Taishan Scholar Professorship (TSHW20091007) tenured at University of Jinan.

References

[1] H. Huang, H. Gong, C.L. Chow, J. Guo, T.J. White, M.S. Tse, O.K. Tan, Low-temperature growth of SnO_2 nanorod arrays and tunable n–p–n sensing response of a ZnO/SnO_2 heterojunction for exclusive hydrogen sensors, Adv. Funct. Mater. 21 (2011) 2680–2686.
[2] L.X. Zhang, J.H. Zhao, H.Q. Lu, L. Li, J.F. Zheng, J. Zhang, H. Li, Z.P. Zhu, Highly sensitive and selective dimethylamine sensors based on hierarchical ZnO architectures composed of nanorods and nanosheet-assembled microspheres, Sens. Actuators B 171–172 (2012) 1101–1109.
[3] G. Yamamoto, T. Yamashita, K. Matsuo, T. Hyodo, Y. Shimizu, Effects of polytetrafluoroethylene or polyimide coating on H_2 sensing properties of anodized TiO_2 films equipped with Pd–Pt electrodes, Sens. Actuators B 183 (2013) 253–264.
[4] (a) H.Y. Xu, X.Q. Chen, J. Zhang, J.Q. Wang, B.Q. Cao, D.L. Cui, NO_2 gas sensing with SnO_2–ZnO/PANI composite thick film fabricated from porous nanosolid, Sens. Actuators B 176 (2013) 166–173;
(b) H.Y. Xu, X.L. Liu, D.L. Cui, M. Li, M.H. Jiang, A novel method for improving the performance of ZnO gas sensors, Sens. Actuators B 114 (2006) 301–307.
[5] X.H. Liu, J. Zhang, L.W. Wang, T.L. Yang, X.Z. Guo, S.H. Wu, S.R. Wang, 3D hierarchically porous ZnO structures and their functionalization by Au nanoparticles for gas sensors, J. Mater. Chem. 21 (2011) 349–356.
[6] Z.P. Fu, Z. Wang, B.F. Yang, Y.L. Yang, H.W. Yan, L.S. Xia, Shape-control of nano-ZnO by changing the solvent, Mater. Lett. 61 (2007) 4832–4835.
[7] Z. Qin, Y.H. Huang, J.J. Qi, H. Feng, L.J. Su, Y. Zhang, Facile synthesis and photoelectrochemical performance of the bush-like ZnO nanosheets film, Solid State Sci. 14 (2012) 155–158.
[8] J. Kim, K. Yong, Mechanism study of ZnO nanorod-bundle sensors for H_2S gas sensing, J. Phys. Chem. C 115 (2011) 7218–7224.
[9] F.T. Liu, S.F. Gao, S.K. Pei, S.C. Tseng, C.J. Liu, ZnO nanorod gas sensor for NO_2 detection, J. Taiwan Inst. Chem. Eng. 40 (2009) 528–532.
[10] N.D. Khoang, H.S. Hong, D.D. Trung, N.V. Duy, N.D. Hoa, D.D. Thinh, N.V. Hieu, On-chip growth of wafer-scale planar-type ZnO nanorod sensors for effective detection of CO gas, Sens. Actuators B 181 (2013) 529–536.
[11] M.W. Ahn, K.S. Park, J.H. Heo, D.W. Kim, K.J. Choi, J.G. Park, On-chip fabrication of ZnO nanowire gas sensor with high gas sensitivity, Sens. Actuators B 138 (2009) 168–173.
[12] Y.J. Chen, C.L. Zhu, G. Xiao, Ethanol sensing characteristics of ambient temperature sonochemically synthesized ZnO nanotubes, Sens. Actuators B 129 (2008) 639–642.
[13] M.S. Yao, P. Hu, Y.B. Cao, W.C. Xiang, X. Zhang, F.L. Yuan, Y.F. Chen, Morphology-controlled ZnO spherical nanobelt-flower arrays and their sensing properties, Sens. Actuators B 177 (2013) 562–569.
[14] L.W. Wang, Y.F. Kang, X.H. Liu, S.M. Zhang, W.P. Huang, S.R. Wang, ZnO nanorod gas sensor for ethanol detection, Sens. Actuators B 162 (2012) 237–243.
[15] W.B. Wu, G.d. Hu, S.G. Cui, Y. Zhou, H.T. Wu, Epitaxy of vertical ZnO nanorod arrays on highly (0 0 1)-oriented ZnO seed monolayer by a hydrothermal route, Cryst. Growth Des. 8 (2008) 4014–4020.
[16] J. Zhang, S.R. Wang, M.J. Xu, Y. Wang, B.L. Zhu, S.M. Zhang, W.P. Huang, S.H. Wu, Hierarchically porous ZnO architectures for gas sensor application, Cryst. Growth Des. 9 (2009) 3532–3537.
[17] Y. Cao, E. Galoppini, P.I. Reyes, Z.Q. Duan, Y.C. Lu, Morphology effects on the biofunctionalization of nanostructured ZnO, Langmuir 28 (2012) 7947–7951.
[18] D. Padilla-Rueda, J.M. Vadillo, J.J. Laserna, Room temperature pulsed laser deposited ZnO thin films as photoluminescence gas sensors, Appl. Surf. Sci. 259 (2012) 806–810.
[19] L.J. Bie, X.N. Yan, J. Yin, Y.Q. Duan, Z.H. Yuan, Nanopillar ZnO gas sensor for hydrogen and ethanol, Sens. Actuators B 126 (2007) 604–608.
[20] Y. Zeng, L. Qiao, Y.F. Bing, M. Wen, B. Zou, W.T. Zheng, T. Zhang, G.T. Zou, Development of microstructure CO sensor based on hierarchically porous ZnO nanosheet thin films, Sens. Actuators B 173 (2012) 897–902.
[21] Z.H. Jing, J.H. Zhan, Fabrication and gas-sensing properties of porous ZnO nanoplates, Adv. Mater. 20 (2008) 4547–4551.
[22] H.N. Chen, W.P. Li, H.C. Liu, L.Q. Zhu, CdS quantum dots sensitized single- and multi-layer porous ZnO nanosheets for quantum dots-sensitized solar cells, Electrochem. Commun. 13 (2011) 331–334.
[23] U.N. Maiti, K.K. Chattopadhyay, S. Karan, B. Mallik, Synthesis of a zinc oxide nanosheet–nanowire network complex by a low-temperature chemical route: efficient UV detection and field emission property, Scr. Mater. 62 (2010) 305–308.

[24] W. Bai, X. Zhu, Z.Q. Zhu, J.H. Chu, Synthesis of zinc oxide nanosheet thin films and their improved field emission and photoluminescence properties by annealing processing, Appl. Surf. Sci. 254 (2008) 6483–6488.
[25] Z.L. Wang, X.Y. Kong, J.M. Zuo, Induced growth of asymmetric nanocantilever arrays on polar surfaces, Phys. Rev. Lett. 91 (2003) 185502.
[26] A. Rahm, G.W. Yang, M. Lorenz, T. Nobis, J. Lenzner, G. Wagner, M. Grundmann, Two-dimension al ZnO:Al nanosheets and nanowalls obtained by Al_2O_3-assisted carbothermal evaporation, Thin Solid Films 486 (2005) 191–194.
[27] L.X. Zhang, J.H. Zhao, H.Q. Lu, L. Li, J.F. Zheng, H. Li, Z.P. Zhu, Facile synthesis and ultrahigh ethanol response of hierarchically porous ZnO nanosheets, Sens. Actuators B 161 (2012) 209–215.
[28] H.T. Fan, Y. Zeng, H.B. Yang, X.J. Zheng, L. Liu, T. Zhang, Preparation and gas sensitive properties of ZnO–CuO nanocomposites, Acta Physicochim. Sin. 24 (2008) 1292–1296.
[29] K. Govender, D.S. Boyle, P.B. Kenway, P.J. Obrien, Understanding the factors that govern the deposition and morphology of thin films of ZnO from aqueous solution, J. Mater. Chem. 14 (2004) 2575–2591.
[30] F.S. Tsai, S.J. Wang, Enhanced sensing performance of relative humidity sensors using laterally grown ZnO nanosheets, Sens. Actuators B 193 (2014) 280–287.
[31] N.D. Khoang, D.D. Trung, N.V. Duy, N.D. Hoa, N.V. Hieu, Design of SnO_2/ZnO hierarchical nanostructures for enhanced ethanol gas-sensing performance, Sens. Actuators B 174 (2012) 594–601.
[32] A. Yu, J.S. Qian, H. Pan, Y.M. Cui, M.G. Xu, L. Tu, Q.L. Chai, X.F. Zhou, Micro-lotus constructed by Fe-doped ZnO hierarchically porous nanosheets: preparation, characterization and gas sensing property, Sens. Actuators B 158 (2011) 9–16.
[33] Z.K. Bai, C.S. Xie, M.L. Hu, S.P. Zhang, D.W. Zeng, Effect of humidity on the gas sensing property of the tetrapod-shaped ZnO nanopowder sensor, Mater. Sci. Eng. B 149 (2008) 12–17.
[34] H.S. Hong, D.T. Phan, G.S. Chung, High-sensitivity humidity sensors with ZnO nanorods based two-port surface acoustic wave delay line, Sens. Actuators B 171–172 (2012) 1283–1287.
[35] J. Xie, H. Wang, Y.H. Lin, Y. Zhou, Y.P. Wu, Highly sensitive humidity sensor based on quartz crystal microbalance coated with ZnO colloid spheres, Sens. Actuators B 177 (2013) 1083–1088.
[36] R.C. Singh, O. Singh, M.P. Singh, P.S. Chandi, Synthesis of zinc oxide nanorods and nanoparticles by chemical route and their comparative study as ethanol sensors, Sens. Actuators B 135 (2008) 352–357.
[37] S.L. Bai, L.Y. Chen, D.Q. Li, W.S. Yang, P.C. Yang, Z.Y. Liu, A.F. Chen, C.C. Liu, Different morphologies of ZnO nanorods and their sensing property, Sens. Actuators B 146 (2010) 129–137.
[38] R.C. Singha, O. Singha, M.P. Singh, P.S. Chandic, Synthesis of zinc oxide nanorods and nanoparticles by chemical route and their comparative study as ethanol sensors, Sens. Actuators B 135 (2008) 352–357.
[39] K.M. Kim, H.R. Kim, K. Choi, H.J. Kim, J.H. Lee, ZnO hierarchical nanostructures grown at room temperature and their C_2H_5OH sensor applications, Sens. Actuators B 155 (2011) 745–751.
[40] T.J. Hsueh, C.L. Hsu, S.J. Chang, I.C. Chen, Laterally grown ZnO nanowire ethanol sensors, Sens. Actuators 126 (2007) 473–477.
[41] N.V. Hieu, N.D. Chien, Low-temperature growth and ethanol-sensing characteristics of quasi-one-dimensional ZnO nanostructures, Sens. Actuators 403 (2008) 50–56.
[42] Z.J. Wang, Z.Y. Li, J.H. Sun, H.N. Zhang, W. Wang, W. Zheng, C. Wang, Improved hydrogen monitoring properties based on p-NiO/n-SnO_2 heterojunction composite nanofibers, J. Phys. Chem. C 114 (2010) 6100–6105.
[43] A. Kolmakov, Y. Zhang, G. Cheng, M. Moskovits, Detection of CO and CO_2 using tin oxide nanowire sensors, Adv. Mater. 15 (2003) 997–1000.
[44] H. Huang, O.K. Tan, Y.C. Lee, T.D. Tran, M.S. Tse, X. Yao, Semiconductor gas sensor based on tin oxide nanorods prepared by plasma-enhanced chemical vapor deposition with postplasma treatment, Appl. Phys. Lett. 87 (2005) 163123–163125.
[45] W. Mokwa, D. Kohl, G. Heiland, Decomposition of ethanol and acetaldehyde on clean ZnO prism and oxygen faces, Surf. Sci. 117 (1982) 659–667.
[46] S. Park, H. Ko, S. An, W.I. Lee, S. Lee, C. Lee, Synthesis and ethanol sensing properties of CuO nanorods coated with In_2O_3, Ceram. Int. 39 (2013) 5255–5262.
[47] T. Jinkawa, G. Sakai, J. Tamaki, N. Miura, N. Yamazoe, Relationship between ethanol gas sensitivity and surface catalytic property of tin oxide sensors modified with acidic or basic oxides, J. Mol. Catal. A: Chem. 155 (2000) 193–200.
[48] D. Zhang, S. Chava, C. Berven, S.K. Lee, R. Devitt, V. Katkanant, Experimental study of electrical properties of ZnO nanowire random networks for gas sensing and electronic devices, Appl. Phys. A 100 (2010) 145–150.
[49] J.Q. Xu, Y.P. Chen, D.Y. Chen, J.N. Shen, Hydrothermal synthesis and gas sensing characters of ZnO nanorods, Sens. Actuators B 113 (2006) 526–531.
[50] X.L. Cheng, H. Zhao, L.H. Huo, S. Gao, J.G. Zhao, ZnO nanoparticulate thin film: preparation, characterization and gas-sensing property, Sens. Actuators B 102 (2004) 248–252.
[51] X.L. Cheng, Y.M. Xu, Z. Cai, L.H. Huo, S. Gao, H. Zhao, Preparation and gas-sensing property of ZnO nano-films, Chin. J. Inorg. Chem. 24 (2008) 157–160.
[52] C.H. Jin, H. Kim, S. Park, H.W. Kim, S. Lee, C. Lee, Enhanced ethanol gas sensing properties of SnO_2 nanobelts functionalized with Au, Ceram. Int. 38 (2012) 6585–6590.
[53] D.L. Chen, X.X. Hou, T. Li, L. Yin, B.B. Fan, H.L. Wang, X.J. Li, H.L. Xu, H.X. Lu, R. Zhang, J. Sun, Effects of morphologies on acetone-sensing properties of tungsten trioxide nanocrystals, Sens. Actuators B 153 (2011) 373–381.

Biographies

Dianxing Ju is currently studying for the M.S. degree in the Department of Material Science and Engineering, University of Jinan, China. Now his research interests focus on the nanostructured materials for the gas sensor applications.

Hongyan Xu received her Ph.D. degree from State Key Lab of Crystal Materials, Shandong University in 2006. Now she is an Associate Professor at School of Materials Science and Engineering, University of Jinan. Her main research interests are the synthesis and fabrication of semiconductor nano-materials and high performance conductive polymer composite chemical gas sensors.

Jun Zhang received his Ph.D. degree from the Department of Chemistry, Nankai University in 2011. Now he is working at School of Materials Science and Engineering, University of Jinan. His research is focused on gas sensing materials.

Jing Guo is currently studying for the M.S. degree in the Department of material science and Engineering, University of Jinan, China. Now her research interests the inorganic semiconductors materials for the gas sensor applications.

Bingqiang Cao received the Ph.D. degree from the Institute of Solid State Physics, Chinese Academy of Sciences (CAS) in 2006. After that, he worked as a postdoctoral researcher at University of Leipzig from September 2006 to August 2008, and then as a JSPS fellow at Kyushu University from August 2008 to July 2009. He then joined the faculty of University of Jinan in China as a Principle Investigator and Oversea Taishan Scholar endowed professor. His research is focused on nanostructures, heterostructures, thin films, and transparent optoelectrical devices based on inorganic semiconductors.